Enhanced Capacitance and Rate Capability of Nanocrystalline VN as Electrode Materials for Supercapacitors

Dong Shu[1,2,4], Cuijuan Lv[1], Fukui Cheng[1], Chun He[3], Kun Yang[1], Junmin Nan[1,2,4], Lu Long[1]*

[1]School of Chemistry and Environment, South China Normal University, Guangzhou 510006, P. R. China
[2]Base of Production, Education & Research on Energy Storage and Power Battery of Guangdong Higher Education Institutes, Guangzhou 510006, P. R. China
[3]School of Environmental Science and Engineering, Sun Yat-sen University, Guangzhou 510275, P. R. China
[4]Key Laboratory of Electrochemical Technology on Energy Storage and Power Generation of Guangdong Higher Education Institutes, South China Normal University, Guangzhou 510006, P. R. China
[*]E-mail: hechun@mail.sysu.edu.cn

Nanocrystalline VN was synthesized from the melamine reduction of V_2O_5 xerogel under a N_2 atmosphere for supercapacitors. The structure, particle size and surface elemental composition are characterized by X-ray diffraction spectroscopy (XRD), nitrogen adsorption/desorption at 77 K, transmission electron microscopy (TEM), Fourier transform infrared spectroscopy (FTIR), X-ray photoelectron spectroscopy (XPS). The electrochemical characterizations were performed by cyclic voltammetry (CV), galvanostatic charge-discharge (CD) test and the electrochemical impedance spectroscopy (EIS) measurements. The XRD result indicates that the nanocrystalline VN belongs to the cubic crystal system. TEM images show the disperse nanocrystalline VN particles. FTIR and XPS results reveal that change in the oxide on nanocrystalline VN surface was the main factor leading to the electrochemical cycling-induced capacitance loss. In addition, the electrochemical results show that the nanocrystalline VN displayed exciting supercapacitive behaviors. A maximum specific capacitance of 413 F g^{-1} was recorded at the current density of 1 A g^{-1}. A respectable rate capability was exhibited by the nanocrystalline VN electrode, showing about 88% of its maximal capacitance at a current load of 4 A g^{-1}. The experimental results indicate that the nanocrystalline VN is promising electrode material for electrochemical supercapacitors.

Keywords: Nanocrystalline VN; Specific capacitance; Vanadium oxide film; Supercapacitor

1. INTRODUCTION

As an auxiliary device for battery, supercapacitor can deliver high power in an instant and has long cycle-lives compared with battery [1-4], and it has been widely applied in many fields, such as consumer electronics, memory back-up devices, portable electronics, and hybrid electric vehicles [5,6].

Generally, depending on the charge-storage mode, supercapacitors are classified into two major types: electrical double-layer capacitors (EDLCs), which utilize the charge storage by adsorption of ions at the surface of electrodes, and pseudocapacitors, which store mostly energy by the presence of fast, reversible Faradic redox reactions between the electrodes and the ions in the appropriate potential window [1]. For EDLCs, nanoporous carbons remain the most employed materials due to their low cost, good electrical conductivity and high surface area [7,8]. On the other hand, many transition metal oxides were used as electrode materials for pseudocapacitors. Hydrous RuO_2 is currently a benchmark pseudocapacitive material [1,9]. It exhibits high specific capacitance value exceeding 1000 F g^{-1}. But its high cost and toxic nature restrict its commercial application. In contrast, NiO_x [10,11], MnO_2 [12-14] and V_2O_5 [15,16] etc. show the advantages of low cost, environmental safety and high theoretical specific capacitance and have been applied extensively in pseudocapacitors. However, one of the main conclusions about these materials are the lack of electronic conductivity compared to RuO_2, which severely limits the practical capability of such oxides based electrodes, especially at a fast scan rate or a high current density during the charge-discharge process.

Therefore, current research efforts are directed to finding cheaper and better electrical conductivity materials for supercapacitors. In this sense, transition metal nitrides such as molybdenum nitrides (MoN and Mo_2N) [17], titanium nitride (TiN) [18] and vanadium nitride (VN) [19-27] have been tested as electrode materials due to their low cost, corrosion resistance and excellent electronic conductivity. VN is considered to be one of the more promising materials. Theoretically, high electronic conductivity of VN ($\sigma_{bulk} = 1.67 \times 10^6 \ \Omega^{-1} \ m^{-1}$) [20] and various oxidation states (II~V) of vanadium are beneficial to its high rate charge-discharge and electrochemical capacitance. Indeed, VN electrodes have demonstrated impressive pseudocapacitance. It was reported that Choi et al [19,20] synthesized nanocrystalline VN by a low-temperature route based on a two-step ammonolysis reaction of VCl_4 in anhydrous chloroform. An impressive specific capacitance of 1340 F g^{-1}, even exceeding that of RuO_2, was obtained for the nanocrystalline VN at a scan rate of 2 mV s^{-1} in 1 M KOH electrolyte. However, the high reactivity and toxicity of VCl_4 required special working conditions (a glovebox and a glovebag) which probably increase cost of production. Compared to above procedure, temperature programmed ammonia reduction of V_2O_5 appears to be a more convenient synthesis to produce VN materials for supercapacitors. Our group [21] synthesized VN powder by calcining V_2O_5 xerogel in a furnace under an anhydrous NH_3 atmosphere. The results showed that VN exhibited acceptable supercapacitive behaviors. The specific capacitance of their VN materials was 161 F g^{-1} in 1 M KOH at the scan rate of 30 mV s^{-1}. Glushenkov et al [22] prepared nanocrystalline VN from the reduction of V_2O_5 powder by ammonia. The specific capacitance of their VN materials was 186 F g^{-1} in 1 M KOH at 1 A g^{-1}. Lately, Porto et al. [23] obtained VO_xN_y samples from the ammonolysis reactions of commercial V_2O_5 and VO_2 precursors, the VO_xN_y samples specific capacitance value was 80 F g^{-1}.

However, it should be noted that VN materials which were synthesized by simple ammonia reduction of V_2O_5 performed a lower capacitance compared to Choi's procedure. And their low specific capacitances may be ascribed to the low specific surface areas of VN and VO_xN_y materials. So in order to overcome the issue, Ghimbeu et al [24] synthesized VN/CNTs nanocomposites from the reduction of V_2O_5/CNTs by ammonia. They expected that the presence of high conductivity, high surface area and high purity carbon nanotubes (CNTs) in the active electrode could lead to an improvement of the electrochemical properties of VN. However, the best capacitance of their nanocomposites was 171 F g^{-1} in 6 M KOH at the scan rate of 2 mV s^{-1} which was only a little better than that of VN materials without CNTs (152 F g^{-1}). Recently, some more innovative methods have been used for preparing VN materials. For example, Zhang et al [25] synthesized three-dimensional arrays of vanadium nitride functionalized carbon nanotubes via physical vapor deposition. They reported that their nanostructures demonstrated a specific capacitance of 289 F g^{-1} at 20 mV s^{-1} and displayed a cycling performance that the specific capacitance values remained at 64% of the original values after 600 CV cycles at 50 mV s^{-1} in 1 M KOH. Dong et al [26] synthesized TiN/VN core-shell composites by a two-step strategy involving coating of commercial TiN nanoparticles with $V_2O_5 \cdot nH_2O$ sols followed by ammonia reduction, and the best capacitance of their composites was 170 F g^{-1} at 2 mV s^{-1}. Zhou et al [27] prepared TiN/VN core-shell nanostructure fibers by the coaxial electrospinning, their fibers exhibited a specific capacitance of 247.5 F g^{-1} at 2 mV s^{-1} and performed an cycle ability that about 88% of original capacitance was retained after 500 cycles at 100 mV s^{-1} in 1 M KOH.

However, although they do a lot of efforts, the rate capability of the VN materials has indeed improved, but they rarely reported the cycling performance of VN materials, probably implying the unsatisfactory cycling performance of their materials. However, Choi [20] reported that the nanocrystalline VN displayed a respectable cycling performance. The specific capacitance values maintained about 90% of the initial values after 1000 cycles. We believe that change of vanadium oxides phase and re-aggregation of the VN nanoparticles during the circulation process make deterioration of the VN material cycle performance. So, to overcome this problem, one of the key issues is developing a synthesis method to produce VN materials with less prone to agglomeration and higher specific surface areas. Consequently, we considered to using organic nitride as nitrogenized reagent to prepare appropriate VN materials.

To prepare VN materials with less prone to agglomeration and higher specific surface areas, a proper precursor of vanadium source and nitrogenized reagent are very important [28,29]. As the precursor, V_2O_5 as a major vanadium source which already mentioned above with relatively low melting point (690 ^{o}C) maybe result in the cohesion and aggregation during the formation of nanocrystalline VN and lead to VN materials with low specific area. As the organic nitridizing reagent, melamine decomposed and released gas during calcination process can prevent the cohesion and aggregation of V_2O_5 precursor and nanocrystalline VN, the carbon remains after melamine decomposition is beneficial to separate nanocrystalline VN particles and improve the electrochemical characteristic of the VN materials. Recently, Cheng et al [30] synthesized nanocrystalline VN by calcining a mixture of melamine and V_2O_5 xerogel at 800 ^{o}C under a N_2 atmosphere. The specific capacitance reached to 273 F g^{-1} in 1 M KOH at the scan rate of 30 mV s^{-1}. This is a considerable

capacitance value. So it was clear that using organic nitrogen as nitride reagents to prepare VN materials indeed improved the electrochemical properties of the material. Their results also proved that the organic precursors play important role in small particle formation.

In this article, nanocrystalline VN was synthesized from the melamine reduction of V_2O_5 xerogel under a N_2 atmosphere at 800 ^{o}C in a furnace. The melamine served as the nitridizing reagent. The physical characteristics of nanocrystalline VN will be investigated depending on X-ray diffraction and transmission electron microscopy. The electrochemical characterization and mechanism of nanocrystalline VN will be discussed in detail in this paper basing on the cyclic voltammetry, galvanostatic charge-discharge tests, Fourier transform infrared spectra, X-ray photoelectron spectroscopy and electrochemical impedance spectroscopy.

2. EXPERIMENTAL

2.1. Material synthesis

Nanocrystalline VN was prepared by calcining a mixture of melamine and V_2O_5 xerogel at 800 ^{o}C under N_2 atmosphere in a furnace. V_2O_5 xerogel was prepared as following. Typically, the V_2O_5 powder was dissolved in H_2O_2 at 0 ^{o}C due to the high exothermicity of the reaction. The solution was stirred for about 2 h, and the remaining H_2O_2 was decomposed by sonication. The as-prepared suspension was aged for 24 h until the dark-brown gels were formed. The gels were dried under vacuum at 50 ^{o}C for 36 h. The V_2O_5 xerogel was ground into fine particles and then mixed with melamine with a weight ratio of 1:20 by ball mill. The mixture was heated up to 800 ^{o}C at the rate of 5 ^{o}C min^{-1} under a nitrogen atmosphere and kept at 800 ^{o}C for 3 h. Finally, the as-prepared sample was achieved.

2.2. Material characterization

The crystalline phase of the synthesized as-prapared VN powers was determined by X-ray diffraction spectroscopy (XRD, BRUKER D8 ADVANCE, Bruker, Germany). The morphology of the powers was observed by transmission electron microscopy (TEM, JSM-2010, JEOL Ltd., Japan). The surface area and pore size distribution were analysed using N_2 adsorption/desorption at 77 K (ASAP-2020, Micromeritics, America). The surface area was calculated from the N_2 adsorption isotherm using the Branauer-Emmett-Teller (BET) equation, and the pore size distribution was determined from Barrett-Joiner-Helenda (BJH) method. The Fourier transform infrared spectroscopy (FTIR, IR-prestige21, Shimadzu Co., Japan) was recorded from KBr pellets. The elemental composition on the surface of as-prepared VN materials was analyzed by X-ray photoelectron spectroscopy (XPS, ESCALAB 250, Thermo Fisher Scientific Co., America).

2.3. Electrochemical Cells Fabrication and Measurements

Three-electrode cells that consisted of a working electrode, a platinum plate counter electrode, and an Hg/HgO as reference electrode were assembled to assess the electrochemical properties of the as-prepared VN materials. The working electrode was prepared by mixing the as-prepared VN materials, acetylene black, graphite and poly (vinylidene fluoride) (PVDF) in N-methylpyrrolidinone (NMP) with a weight ratio of 75:10:10:5. The cyclic voltammetry (CV) and galvanostatic charge-discharge (CD) tests were performed by a CHI 660A electrochemical working station in 1 M KOH aqueous electrolytes at room temperature. EIS tests were carried out using the frequency range from 10^{-2} Hz to 100 kHz by an Autolab PGSTAT30. The specific capacitance (SC), in farads per gram, based on CV and CD can be calculated by the following equations:

$$SC_{CV} = \frac{Q}{m\Delta E} \tag{1}$$

$$SC_{CD} = \frac{i\Delta t}{m\Delta E} \tag{2}$$

where Q the integrated cathodic charge, *m* the mass of the active material, ΔE the potential window, *i* the discharge current, and Δt is the discharge time.

3. RESULTS AND DISCUSSIONS
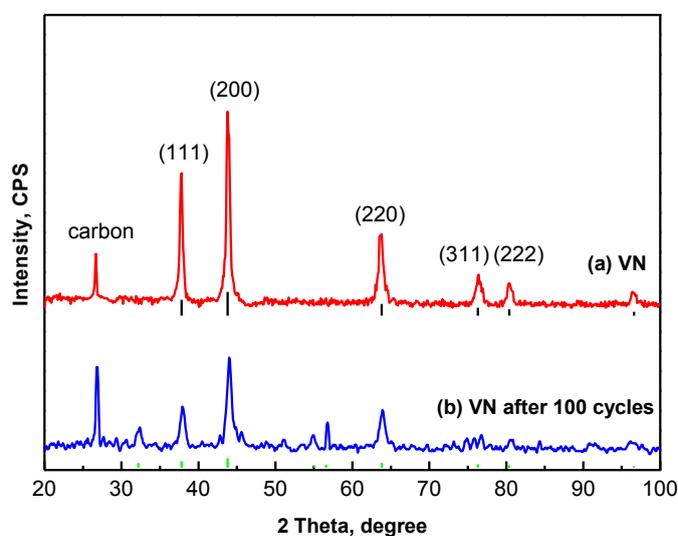
3.1. Structural Characterization

Figure 1. The XRD patterns of VN sample (a) before first cycle; (b) after 100th cycle.

X-ray diffraction spectroscopy (XRD) pattern of the as-prepared VN materials was supplied in Figure 1. As Figure 1 (a) shows, three strong diffraction peaks are observed at 2θ values of 37.8°, 43.8°, and 63.7°, and this XRD pattern can be indexed according to a cubic structure with space group Fm3m and lattice parameter 4.139 Å, corresponding to stoichiometric VN (ICDD PDF 35-768). This three strong diffraction peaks can be ascribed to the (111), (200), and (220) crystal planes. It can be seen that no peaks corresponding to vanadium oxide phase could be detected in the XRD patterns in as-prepared VN materials before electrochemical cycling. Therefore, the presence of large amount of vanadium oxide can be excluded. The peak at around 26.7° indicates the presence of carbon in as-prepared materials.
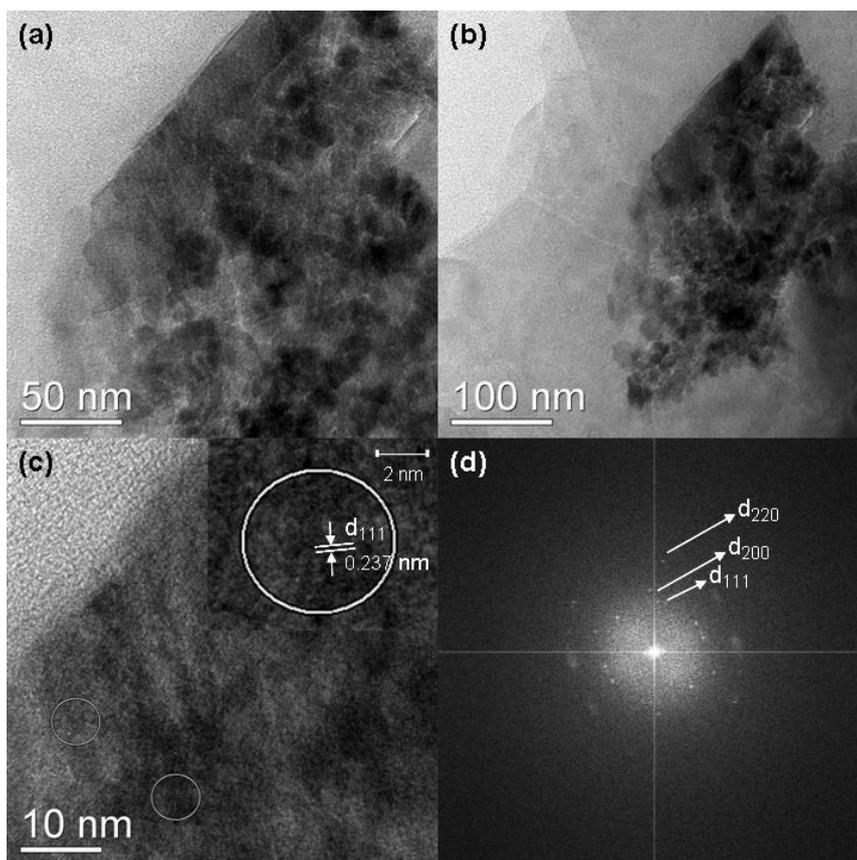

Figure 2. (a and b)TEM images of VN sample; (c) HRTEM image of VN sample, inset shows VN nanocrystals; (d) the corresponding powder spectrum of VN sample.

The transmission electron microscopy (TEM) images of the as-prepared VN can be found in Figure 2. As Figures 2 (a) and (b) show, irregular VN nanoparticles in the range of 10~30 nm are separated by the remained carbon. In other word, the remained carbon disperses among VN nanoparticles and prevents the aggregation and re-crystallization of the VN nanoparticles. Further, we hold opinion that the remained carbon can improve the discharge rated capability of VN during its electrochemical process.

To evaluate more detailed characterization of the as-prepared VN, additional TEM work was conducted in this part. Figure 2 (c) is a high resolution image taken from the as-prepared VN. Figure 2(d) is the corresponding selected area electron diffraction (SAED) pattern. As the Figure 2 (c) and (d) show, the high-resolution image and diffraction circles of nanocrystalline VN are not very clear, indicating a low degree crystallinity of VN, presumably as a result of the deposited carbon. However, a (111) plane of VN was still observed in this part, and it is showed in the high-magnification TEM image in the inset from bottom cycle (Figure 2 (c)). In addition, the SAED pattern displays the nanocrystalline VN diffraction ring pattern. They are the (111), (200) and (220) VN reflections.
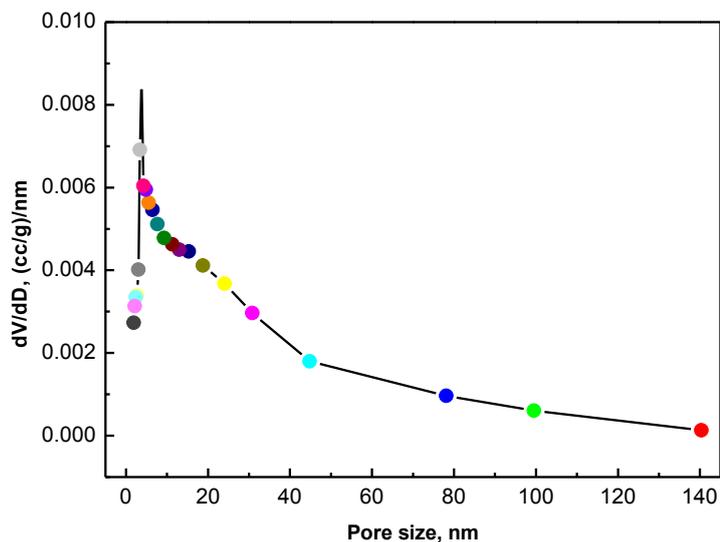

Figure 3. Pore size distribution of the VN sample produced.

The BJH method was used to determine the pore size distribution of the samples. As illustrated in Figure 3, a narrow pore size distribution (5~15 nm) in the range of mesoporosity is observed for the nanocrystalline VN, which yields a specific surface area of 57 m^2 g^{-1}, and it is much larger than the reported values of 38.8 m^2 g^{-1} from VCl_4 [20] and 22.9 m^2 g^{-1} from V_2O_5 [22] reduced by ammonia. As previously discussed, the organic nitrogen reagent is beneficial in the formation of VN with high specific surface area which may further improve the discharge rated capability of VN during its electrochemical process.

3.2. Electrochemical Properties

We reported the electrochemical capacitive performance of the nanocrystalline VN by the melamine reduction of a V_2O_5 xerogel in several different electrolytes. It was found that the VN displayed the best electrochemical capacitive performance in 1 M KOH [30]. Here, we further studied the electrochemical capacitive behavior and its pseudocapacitive mechanism by various analytical methods.

The cyclic voltammetry (CV) measured at various scan rates of 10~100 mV s^{-1} for the nanocrystalline VN is shown in Figure 3 (a). The suitable potential window is defined as -1.1 ~ 0 V (vs. Hg/HgO). As Figure 3 (a) shows, the shape of all the CV curves is quite similar and closes to rectangular mirror images, revealing good electrochemical reversibility for the nanocrystalline VN material. Figure 3 (b) gives the relationship between the specific capacitance and the scan rate. The specific capacitances decreased from 300 to 218 F g^{-1} as the sweep rate was increased from 10 to 100 mV s^{-1}. It is obviously that the capacitance of the nanocrystalline VN in our work is much higher than the value obtained from the reduction of V_2O_5 by ammonia, 161 F g[-1][21],186 F g[-1][22] and 80 F g[-1][23].
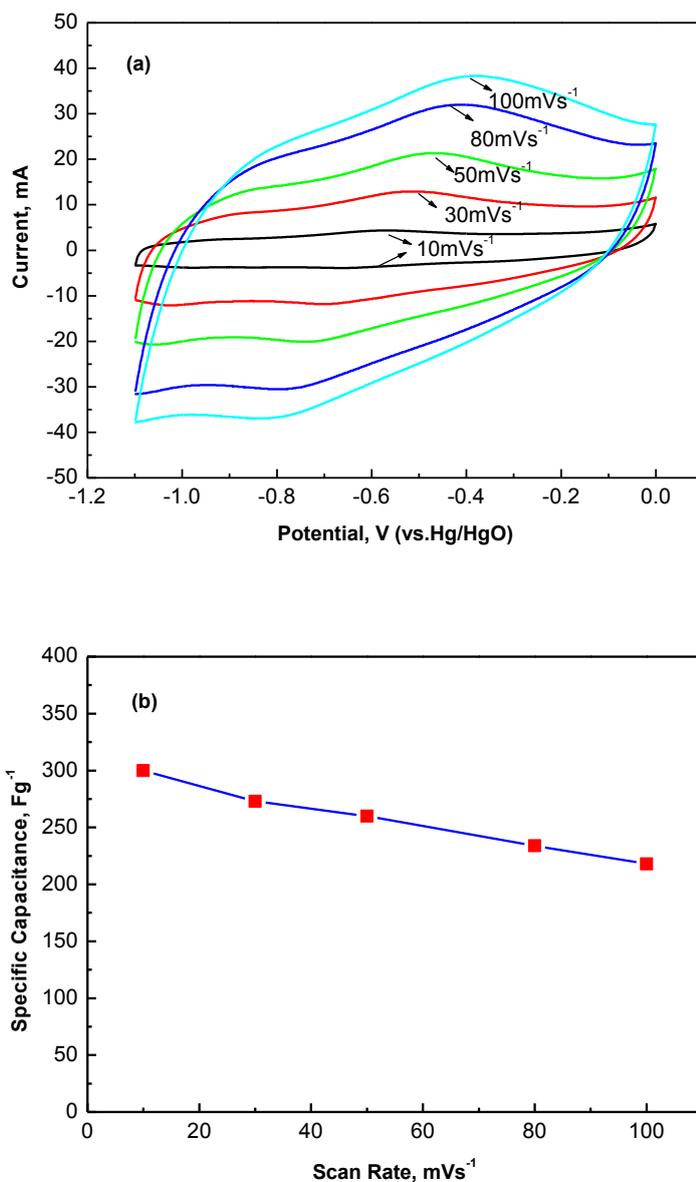

Figure 4. (a) CV curves of nanocrystalline VN at different scan rates in 1 M KOH; (b) the specific capacitance versus scan rate.

Generally, it is suggested that the electrochemical capacitive mechanism of the nanocrystalline VN arises from a combination of the electrical double-layer formation and the faradic redox reactions that occur on the surface of the partially oxidized VN particles, and the higher electrical double-layer capacitance is attributed to its higher specific surface area which can improve the utilization rate of material during the electrochemical process. According to the BET result, the specific surface area ($56.8 \text{ m}^2 \text{ g}^{-1}$) of as-prepared is obviously higher than that of Glushenkov group's ($22.9 \text{ m}^2 \text{ g}^{-1}$) [22]. On the other hand, the pseudo-capacitance which resulted from the Faradic redox reactions on the surface of electrodes is also involved in the electrochemical process. In order to obtain redox potentials which correspond to the pseudocapacitance behavior, CV experiment is conducted on the VN at a lower scan rate of 10 mV s^{-1}, and the CV curve is shown in Figure 4. As can be seen, three pairs of distinguishable redox peaks appear near -0.91, -0.57, and -0.23 V during charging, and -0.98, -0.64, and -0.32 V during discharging, confirming the fast Faradic reaction on the surface of the nanocrystalline VN materials. These results indicate that the nanocrystalline VN electrode exhibits excellent pseudocapacitance behavior. Furthermore, Figure 3 (b) also shows that the specific capacitive reserves about 73% when the scan rate increases 10 times from 10 to 100 mV s^{-1}, indicating that the nanocrystalline VN has a pleasing rate discharge capability. Overall, the nanocrystalline VN shows desirable specific capacitance and rate discharge capability.
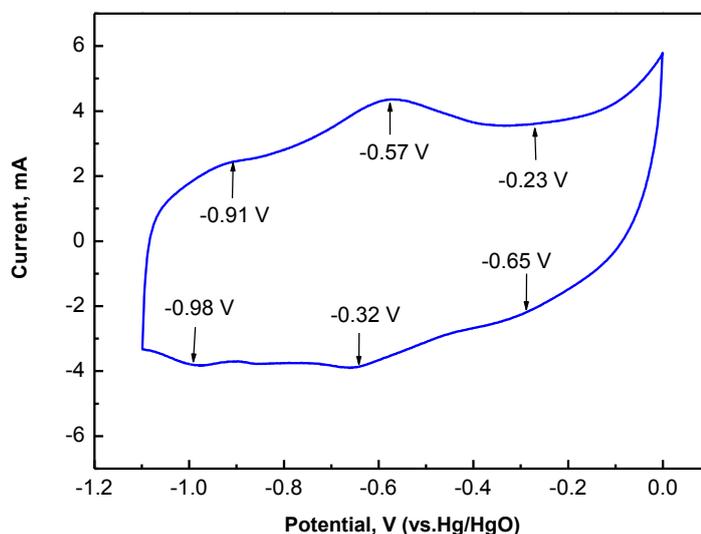

Figure 5. CV curve of nanocrystalline VN at the scan rate of 10 mV s^{-1} in 1 M KOH.

The galvanostatic charge-discharge (CD) test is considered to be an alternative and arguably better quantitative method to evaluate the supercapacitive nature of an electrode material compared to the CV measurement [1]. The supercapacitive characteristic of the nanocrystalline VN is further analyzed by CD experiment, with current densities from 1 to 4 A g^{-1}, the CD curves are shown in Figure 5, and the capacitance values observed at different potentials are illustrated in Figure 6. As can be seen, the highest specific capacitance of 413 Fg^{-1} is recorded at the current density of 1 A g^{-1} in our work. This is a considerable capacitance value and rarely seen before. In addition, the specific

capacitance degrades gradually from 413 to 344 F g^{-1} as the current density increases from 1 to 4 A g^{-1}, it retains about 88% of its maximal capacitance at a current load of 4 A g^{-1}.
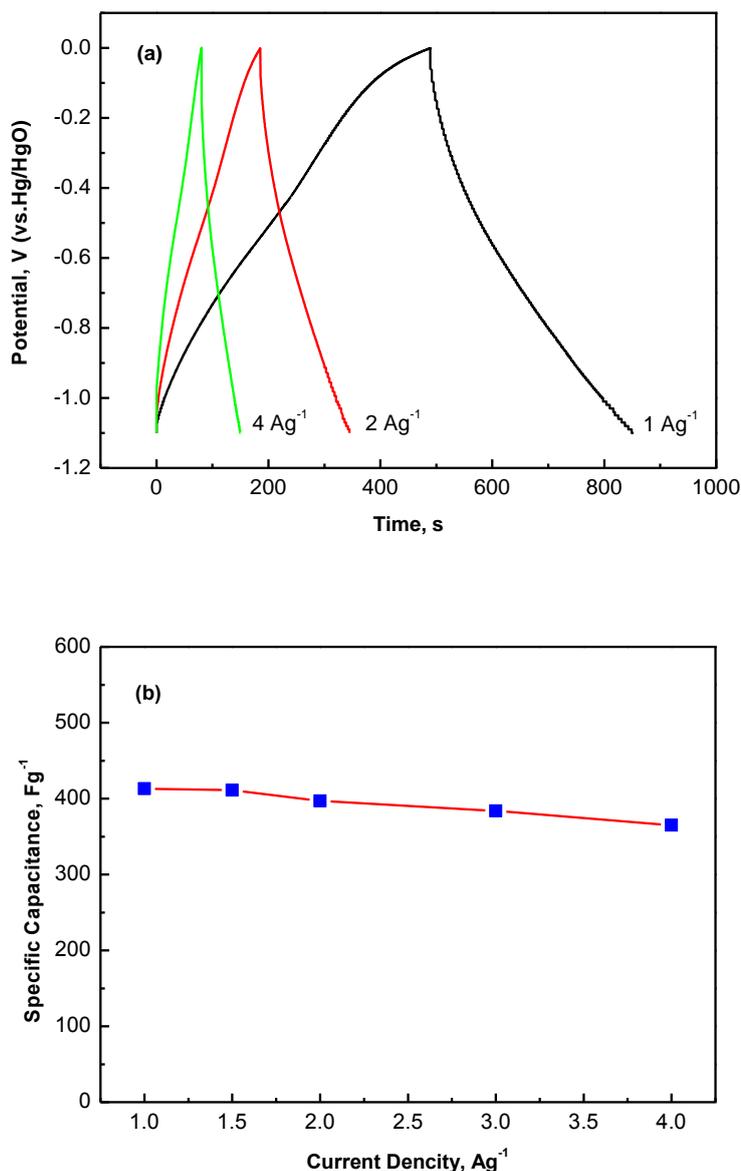
Figure 6. (a) The charge-discharge curves of nanocrystalline VN for varying current densities; (b) specific capacitance versus current density.

It is shown that the nanocrystalline VN electrode maintains a favorable stability during the high power charge-discharge cycling test and demonstrates a respectable rate capability. For the electrode material, good electronic conductivity helps to achieve good capacitance and rate discharge capability. The electronic conductivity of the as-prepared nanocrystalline VN was obtained by four-probe technology, and it was $\sigma_{powder} = 5.8 \times 10^3$ Ω^{-1} m^{-1}, this value is close to Choi group's result ($\sigma_{powder} = 8.2 \times 10^3$ Ω^{-1} m^{-1}) [20], showing the superior conductivity of our nanocrystalline VN. Therefore, it could be suggested that the superior conductivity enhanced the capacitance and rate capability of the

nanocrystalline VN. What is more, it was thought that the electrochemical capacitive performance of VN is also affected by the particle size, specific surface area and the electrochemical conditions, etc [31]. In general, the CD experiments give same electrochemical capacitive performance of VN as CV tests, the higher specific capacitance and rate discharge capability were proved for the nanocrystalline VN materials.

Cycling stability is an important property for a practical supercapacitor. Here, the nanocrystalline VN electrode was subjected to a long-term cycling test.
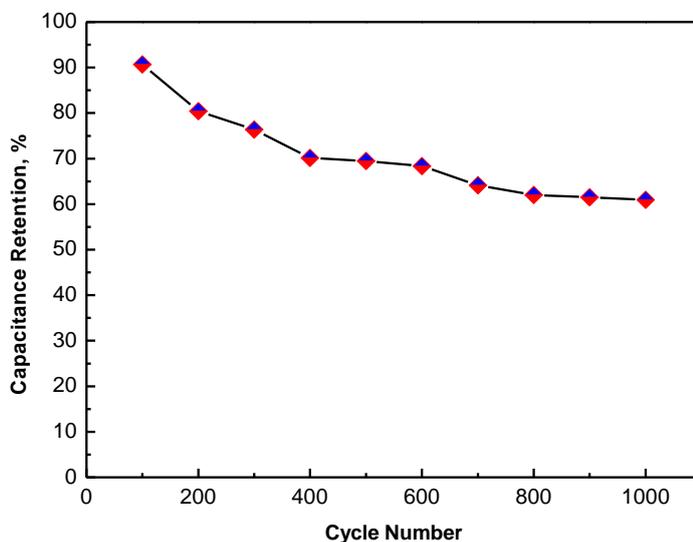

Figure 7. Cyclic behavior of VN nanocrystals scanned at current density of 1 A g^{-1} up to 1000 cycles in 1M KOH.

Figure 7 shows the stability of the nanocrystalline VN. As can be seen, after 1000 CD cycles at current density of 1 A g^{-1}, the specific capacitance values remained about 60% of the initial values, exhibiting an acceptable cycling performance of the nanocrystalline VN materials, but this capability is inferior to that of Choi group's. However, the cycling ability of their VN was strongly dependent upon the electrochemical window used for the electrochemical tests. From their paper, it was known that a large window (-1.2 V up to 0V vs. Hg/HgO) was detrimental to the stability of the electrode. The cycling ability of their VN was improved only when the window limited below -0.3 V for the upper potential cut-off limit. Unfortunately, with a cell voltage limited to 0.9 V the energy density will be restricted. Nevertheless, the cyclic potential window of our nanocrystalline VN is 1.1 V, which wider than that of Choi group's, and the wider potential window would result in the better energy density for a cell.

It was proposed [20] that the cycling performance was determined by several parameters like crystallite size, oxide layer, material loading, electrolyte concentration, and potential window. We believe that change in vanadium oxide layer on the surface of the nanocrystalline VN during the circulation process mainly made deterioration of the VN material cycle performance in 1 M KOH. So in this paper, change in vanadium oxide layer was analyzed by various methods.

Firstly, according to XRD, as Figure 1 illustrated, some peaks appeared at 32.2º, 55.1º and 56.6º after 100 cycles, which can be assigned to vanadium oxides characteristic peaks [16], evidencing vanadium oxides phase formed during electrochemical process. Further explanation, from the pH versus standard hydrogen electrode (SHE) potential diagram provided by Pourbaix and Kelsall et al [32], the stable solid vanadium oxides films observed within the potential range of 0 to -1.2 V in 1 M KOH electrolyte (pH 14) are mainly VO, V_3O_5, or V_2O_3 with the possibility of V_2O_4. So in CD cyclic process, the vanadium oxide film will create or arise from the initial oxide phase and present on the nitride surface, it also will result in poor electronic conductivity. As a conclusion, the gradually produced vanadium oxide film would probably lead to large electronic resistance, and then result in the loss of reversibility.

To further understand the surface chemistry and the electrochemical stability of the nanocrystalline VN in alkaline solution, Fourier transform infrared spectroscopy (FTIR) and X-ray photoelectron spectroscopy (XPS) analyses were carried out on the pre- and post-electrochemically cycled the nanocrystalline VN material.
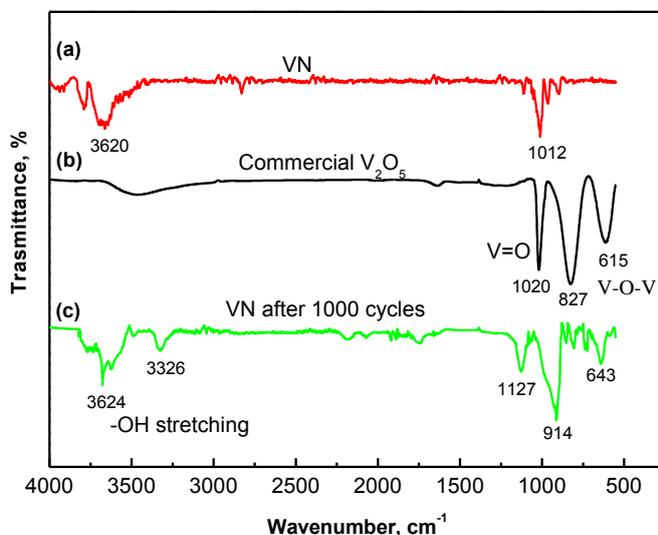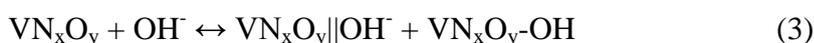

Figure 8. FTIR spectra of (a) nanocrystalline VN; (b) V_2O_5 ; (c) VN after 1000 cycles at 1 A g^{-1}.

The Fourier transform infrared (FTIR) spectra of the nanocrystalline VN (a) before and (c) after 1000 cycles at the current density of 1 A g^{-1} in 1 M KOH are depicted in Figure 8. As Figure 8 shows, a characteristic peak of VN appeared at 3620 cm^{-1} before cycles, which is similar to Choi group's experimental result. Another weak absorption peak at 1012 cm^{-1} confirms the presence of vanadium oxide films on the as-prepared VN surface. In addition, Figure 8 also shows that three absorption peaks were detected at 1127, 914 and 643 cm^{-1} after 1000 cycles which could be conjectured as the characteristic peaks of V=O and V-O-V, respectively. For comparison, the FTIR spectrum of (b) commercial V_2O_5 was also depicted in Figure 8. The absorption of commercial V_2O_5 bands at 1020, 827 and 615 cm^{-1} relate to the stretching vibration absorption peak of V=O, the asymmetric and symmetric stretching vibration absorption peaks of V-O-V, respectively [33]. The

three characteristic peaks which were obtained from the post-electrochemically cycled nanocrystalline VN are clearly blue-shifted comparing with the corresponding crystalline V_2O_5 due to the withdrawing induction and conjugative effect of V≡N group. These could indicate that the oxygen atoms are linked on the VN backbones and various vanadium oxides or bonding sites are created during electrochemical processing in the 1 M KOH electrolyte.

As shown in Figure 8, two peaks appear in 3000~4000 cm^{-1} range after 1000 cycles. The peak at 3326 cm^{-1} corresponds to hydrogen-bonded -OH stretching peak. The peak at 3624 cm^{-1} is blue-shifted comparing with the characteristic peak of VN at 3620 cm^{-1} before cycles. It may correspond to the combination of the free -OH stretching peak and the adsorption of -OH on the VN surface peak. Analysis of the FTIR spectra implies that the -OH group and hydroxyl ions play a key role during the charge-discharge process. Furthermore, CV tests confirm that there are some Faradic reactions on the surface of our nanocrystalline VN materials. Therefore, a possible equilibrium reaction on the nitride or oxy-nitride surface was suggested by Choi group as follows:

$$VN_xO_y + OH^- \leftrightarrow VN_xO_y\|OH^- + VN_xO_y\text{-}OH \qquad (3)$$

where $VN_xO_y\|OH^-$ and VN_xO_y-OH represent the electrical double layer and redox reaction, respectively.

The XPS technique is an effective tool to determine the presence of elements at the surface, estimate their content quantitatively and study the depth profile of elemental composition at the surface of the samples [22]. The chemical nature of our nanocrystalline VN material surface was analyzed by XPS. The oxidation states on the sample surfaces are revealed between the binding energies of 507 and 535 eV, which correspond to the presence of O 1s V, 2p^1 and V 2p^3 peaks. Figure 9 (a) provides the XPS spectra of pre-electrochemically cycled our nanocrystalline VN. The O 1s strong characteristic peak at 530.0 eV is expected for a metal oxide, confirming that a thin oxide layer exists on the surface of the nanocrystalline VN. Similarly, the O 1s characteristic peak reported in ref 20 is also strong although the content of oxygen in their material was small. It suggests that a trace amount of oxygen can also cause a strong peak. Figure 9 (a) also shows the V2p^3 binding energy of 513.4 eV which can be belonged to vanadium in the vanadium nitride structure [22], and the V2p^3 binding energy of 517.1 eV which most likely corresponds to high states of vanadium in the materials [22]. However, when the nanocrystalline VN materials are subjected to electrochemical cycling, as shown in Figure 9 (b), the O 1s peak shifted to 531.8 eV and it is characteristic of a hydroxyl group (-OH) [34], indicating that -OH bonded to the nanocrystalline VN surface during electrochemical cycling. In addition, one of the V2p^3 characteristic peak shifted to 513.7 eV with an increase in intensity that possibly indicates an increase of the relative amounts of -OH nanocrystalline VN surface, and it is close to that of V(OH)$_3$(514.1 eV) [33]. On the other hand, the other V2p^3 characteristic peak shifted to 517.4 eV, with a decrease in intensity that indicates a change in the relative amounts of each oxide during electrochemical cycling. This phenomenon is similar to the Choi group's result which was suggested that a reduction of the V_2O_5-type structure changed into either VO_2 or V_2O_3-type oxides through electron transfer during electrochemical cycling. However, it is difficult to categorically distinguish between these oxides since the binding-energy difference is narrow [22]. As a result, it just can be concluded that, after

electrochemical cycling, the relative amounts of -OH were changed and vanadium oxides such as VO and V_2O_3 which would finally lead to the loss of reversibility presented on the surface of the nanocrystalline VN. And the XPS analysis is similar to that of FTIR and XRD, further evidencing the above equilibrium reaction on the nitride or oxy-nitride surface.
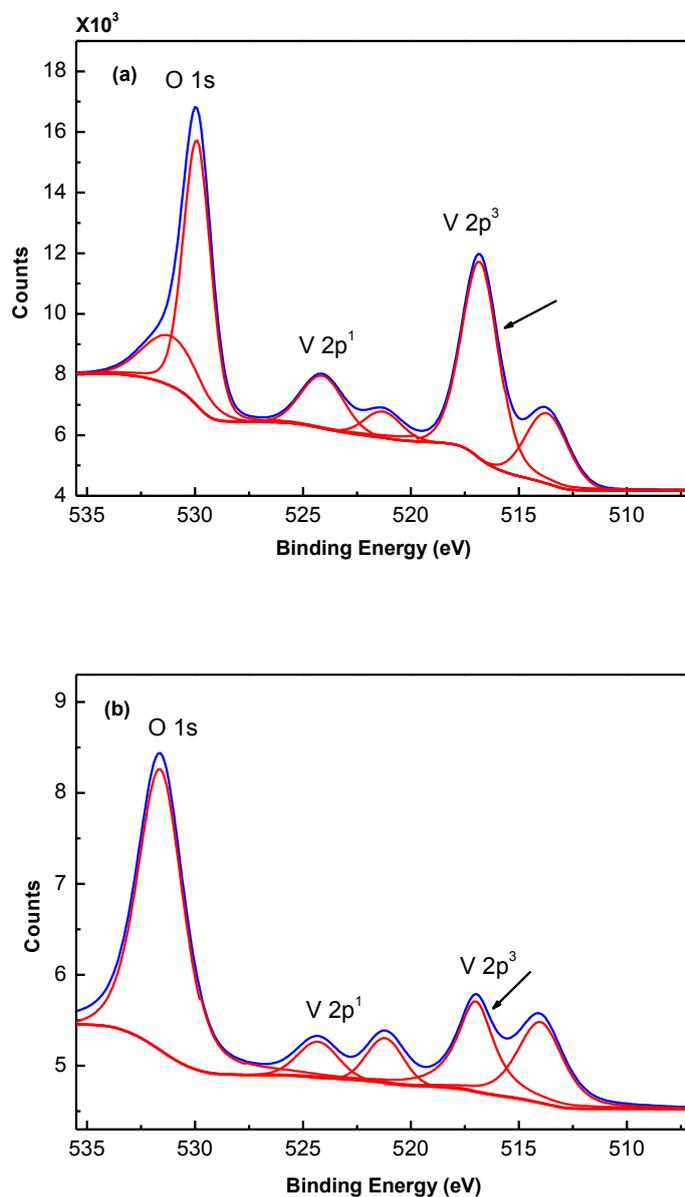
Figure 9. XPS spectra of nanocrystalline VN (a) before first cycle and (b) after 1000th cycle at 1 A g^{-1} in 1 M KOH.

Finally, electrochemical impedance spectroscopy (EIS) measurements were carried out to further verify the performance of our nanocrystalline VN electrode. Figure 10 represents the EIS of the nanocrystalline VN electrode before first and after 1000th cycle, applying 5 mV AC voltages in the frequency range from 0.1 Hz to 100 kHz. The semicircles in the high-frequency range are usually associated with the electrochemical processes of the nanocrystalline VN electrodes, and the diameter

of the semicircles corresponds to the charge-transfer resistance (Rct). The Rct values gained at different potentials were illustrated in Figure 11.
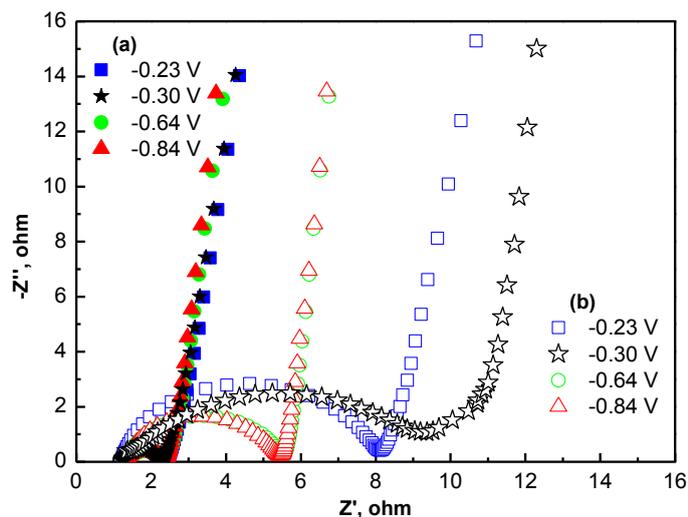

Figure 10. Nyquist plots of the nanocrystalline VN electrode between 10^{-2} and 10^{5} Hz: (a) before first cycle; (b) after 1000th cycle at 1 A g^{-1} in 1 M KOH.
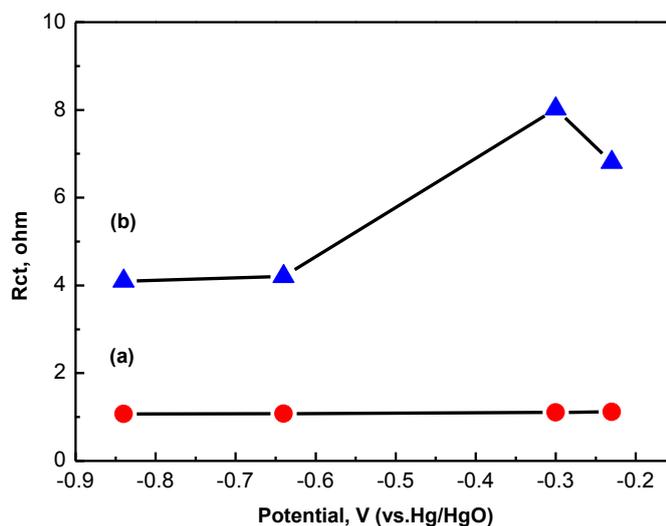

Figure 11. The variation of charge-transfer resistance (Rct) with potential (a) before first cycle and (b) after 1000th cycle at 1 A g^{-1} in 1 M KOH.

It can be seen that low Rct values (~1.1 Ω) were observed before first cycle, implying the excellent conductivity of our nitride material electrode in KOH electrolyte. Figure 11 also shows the Rct values of the nanocrystalline VN electrode after 1000th cycle. As can be seen, the Rct values increase to 4~8 Ω after 1000th cycle, and they locate in about 4.1Ω at low potential (-0.64 V and -0.84 V), but they rise to 6.8 Ω and 8.0 Ω at high potential (-0.23 V and -0.30 V). It is clear that the Rct

values of the nanocrystalline VN electrodes observed at different potentials are all increase after cycling, revealing that a charge transfer reaction is indeed happening during electrochemical cycling. According to the analyses of XRD, FTIR and XPS, the increase of Rct values could be ascribed to the creation of vanadium oxides with poor electric conductivity on the surface of electrode materials during electrochemical cycling. It also can be concluded that the impedance of electrodes is increase after cycling, and the increase impedance leads to the loss of reversibility.

4. CONCLUSIONS

In summary, the nanocrystalline VN was successfully prepared by calcining a mixture of melamine and V_2O_5 xerogel at 800 ^{o}C under a N_2 atmosphere in our work. As the organic nitridizing reagent, melamine decomposed and released gas during calcination process can prevent the cohesion and aggregation of V_2O_5 precursor and nanocrystalline VN, the carbon remains after melamine decomposition is beneficial to separate nanocrystalline VN particles. Series of analyses make known that the nanocrystalline VN exhibited superior supercapacitive behavior in 1 M KOH electrolyte. A maximal specific capacitance of 413 F g^{-1} was demonstrated at current density of 1 A g^{-1}. Moreover, it also showed that the nanocrystalline VN were possessed of a super rate capability, retaining about 88% of its maximal capacitance at a current load of 4 A g^{-1}. XRD, FTIR and XPS analyses confirmed that vanadium oxides presented during cycling. EIS revealed that the impedance of electrode is increase which leads to the loss of reversibility after cycling. Overall, the nanocrystalline VN prepared by using melamine as the nitridizing reagent is a promising active material for supercapacitors. The present synthetic strategy could be extended to other metal nitrides such as molybdenum nitrides and titanium nitrides.

References

1. B.E. Conway, Electrochemical Supercapacitors, Scientific Fundamentals and Technological Applications, Kluwer Academic/Plenum Publications, New York (1999)
2. P. Simon and Y. Gogotsi, *Nature Mater.*, 7 (2008) 845
3. Z. Du, S. Zhang, J. Zhao, T. Jiang and Z. Bai, *Int. J. Electrochem. Sci.*, 7 (2012) 1180
4. G. Han, Z. Ye, C. Cao, B. Liu, B. Li and S. Guan, *Int. J. Electrochem. Sci.*, 7 (2012) 10142
5. J. R. Miller and A. F. Burke, *Electrochem. Soc. Interface*, 17 (2008) 53
6. L.T. Lam and R. Louey, *J. Power Sources*, 158 (2006) 1140
7. M. Inagaki, H. Konno and O. Tanaike, 195 (2010) 7880
8. A.G. Pandolfo and A.F. Hollenkamp, *J. Power Sources*, 157 (2006) 11

9. C. C. Hu, K. H. Chang, M. C. Lin and Y. T. Wu, *Nano Lett*., 6(12) (2006) 2690
10. A. I. Inamdar, Y. S. Kim, S. M. Pawar, J. H. Kim, H. Im and H. Kim, *J. Power Sources*, 196 (2011) 2393
11. J. Chang, M. Park, D. Ham, S.B. Ogale, R. S. Mane and S. H. Han, *Electrochim. Acta*, 53 (2008) 5016
12. H. Zhang, G. Cao, Z. Wang, Y. Yang, Z. Shi and Z. Gu, *Nano Lett*. 8 (9) 2008, 2664.
13. A. Cross, A. Morel, A. Cormie, T. Hollenkamp and S. Donne, *J. Power Sources*, 196 (2011) 7847
14. S. Wang, Q. Liu, J. Yu and J. Zeng, *Int. J. Electrochem. Sci*., 7 (2012) 1242
15. J. Shao, X. Li, Q. Qu and H. Zheng, *J. Power Sources,* 219 (2012) 253
16. G. Wee, H. Z. Soh, Y.L. Cheah, S. G. Mhaisalkar and M. Srinivasan, *J. Mater. Chem*., 20 (2010) 6720
17. T.C. Liu, W. G. Pell and B. E. Conway, *J. Electrochem. Soc*., 145(6) (1998) 1882
18. S. Dong, X. Chen, L. Gu, X. Zhou, H. Xu, H. Wang, Z. Liu, P. Han, J. Yao, L. Wang, G. Cui and L. Chen, *ACS Appl. Mater. Interfaces*, 3(1) (2011) 93
19. D. Choi and P. N. Kumta, *Electrochem. Solid-State Lett*., 8(8) (2005), A418
20. D. Choi, G. E. Blomgren and P.N. Kumta, *Adv. Mater*., 18 (2006) 1178
21. X. Zhou, H. Chen, D. Shu, C. He and J. Nan, *J. Phys. Chem. Solids*, 70 (2009) 495
22. A.M. Glushenkov, D. Hulicova-Jurcakova, D. Llewellyn, G.Q. Lu and Y. Chen, *Chem. Mater*., 22 (2010) 914
23. R. L. Porto, R. Frappier, J. B. Ducros, C. Aucher, H. Mosqueda, S. Chenu, B. Chavillon, F. Tessier, F. Chevire and T. Brousse, *Electrochim. Acta*, 82 (2012) 257
24. C.M. Ghimbeu, E. Raymundo-Pinero, P. Fioux, F. Beguin and C. Vix-Guterl, *J. Mater. Chem*., 21 (2011) 13268
25. L. Zhang, C. M. B. Holt, E. J. Luber, B. C. Olsen, H. Wang, M. Danaie, X. Cui, X. H. Tan, V. W. Lui, W. P. Kalisvaart and D. Mitlin, *J. Phys.Chem. C*, 115 (2011) 24381
26. S. Dong, X. Chen, L. Gu, X. Zhou, H. Wang, Z. Liu, P. Han, J. Yao, L. Wang, G. Cui and L. Chen, *Mater. Res. Bull*., 46 (2011) 835
27. X. Zhou, C. Shang, L. Gu, S. Dong, X. Chen, P. Han, L. Li, J. Yao, Z. Liu, H. Xu, Y. Zhu and G. Cui, *ACS Appl. Mater. Interfaces,* 3 (2011) 3058
28. J. Buha, I. Djerdj, M. Antonietti and M. Niederberger, *Chem. Mater.,* 19(14) (2007) 3499
29. C. Giordano, C. Erpen, W. Yao, B. Milke and M. Antonietti, *Chem. Mater*., 21 (2009) 5136
30. F. Cheng, C. He, D. Shu, H. Chen, J. Zhang, S. Tang and D. E. Finlow, *Mater. Chem. Phys*., 131 (2011) 268
31. S. Peng, N. F. Wang, X.J. Wu, S. Q. Liu, D. Fang, Y. N. Liu and K. L. Huang, *Int. J. Electrochem. Sci.*, 7 (2012) 643
32. G. H. Kelsall, I. Thompson and P. A. Francis, *J. Appl. Electrochem*., 23 (1993) 417
33. J.M. Lee, H. S. Hwang, W. I. Cho, B. W. Cho and K.Y. Kim, *J. Power Sources*, 136 (2004) 122
34. V. Bondarenka, S. Grebinskij, S. Mickevicius, H. Tvardauskas, S. Kaciulis, V. Volkov, G. Zakharova and A. Pasiskevicius, *Lithuanian J. Phys*., 47(3) (2007) 333